LETTERS

Intrinsic functional architecture in the anaesthetized monkey brain

J. L. Vincent[1,5,6], G. H. Patel[1,2,3], M. D. Fox[1], A. Z. Snyder[1,2], J. T. Baker[3], D. C. Van Essen[3], J. M. Zempel[2], L. H. Snyder[3], M. Corbetta[1,2,3] & M. E. Raichle[1,2,3,4]

The traditional approach to studying brain function is to measure physiological responses to controlled sensory, motor and cognitive paradigms. However, most of the brain's energy consumption is devoted to ongoing metabolic activity not clearly associated with any particular stimulus or behaviour[1]. Functional magnetic resonance imaging studies in humans aimed at understanding this ongoing activity have shown that spontaneous fluctuations of the blood-oxygen-level-dependent signal occur continuously in the resting state. In humans, these fluctuations are temporally coherent within widely distributed cortical systems that recapitulate the functional architecture of responses evoked by experimentally administered tasks[2–6]. Here, we show that the same phenomenon is present in anaesthetized monkeys even at anaesthetic levels known to induce profound loss of consciousness. We specifically demonstrate coherent spontaneous fluctuations within three well known systems (oculomotor, somatomotor and visual) and the 'default' system, a set of brain regions thought by some to support uniquely human capabilities. Our results indicate that coherent system fluctuations probably reflect an evolutionarily conserved aspect of brain functional organization that transcends levels of consciousness.

It has been suggested that coherent spontaneous blood-oxygen-level-dependent (BOLD) fluctuations observed in the resting state reflect unconstrained but consciously directed mental activity[7]. Alternatively, coherent BOLD fluctuations may persist in the absence of normal perception and behaviour, reflecting a more fundamental or intrinsic property of functional brain organization. Importantly, the former view predicts that coherent BOLD fluctuations should be absent in the anaesthetized state, in which conscious mental activity is thought to be absent.

We acquired whole-brain BOLD functional magnetic resonance imaging (fMRI) in isoflurane-anaesthetized monkeys and observed highly organized patterns of spontaneous BOLD fluctuations (see Methods). We first examined ongoing fluctuations in the oculomotor system because it is well characterized both functionally and anatomically in the monkey and shows correlated spontaneous BOLD fluctuations in awake resting humans[8]. To explore the spatial distribution of ongoing BOLD fluctuations within the monkey oculomotor system, we correlated the time course of BOLD fluctuations averaged within a priori defined regions of interest (ROIs) around the frontal eye fields (FEF) and the lateral intraparietal area (LIP) with the time course of each voxel within the brain (regions defined from a study of visually guided saccades[9]). Figure 1 shows the distribution of voxels temporally correlated with fluctuations in the right LIP. Correlation maps were computed on the basis of single BOLD runs (15 min each) in one monkey at two levels of isoflurane anaesthesia (A, 0.90%; B, 1.25%) and are shown paired with the simultaneously acquired electroencephalogram (EEG). These traces show continuous slow waves of EEG activity (Fig. 1a) as well as burst–suppression patterns (Fig. 1b), which are characteristic of moderately deep anaesthesia. The principal constituents of the cortical oculomotor system (bilateral FEF and bilateral LIP) are present in the correlation maps at both levels of anaesthesia. These single-subject results demonstrate that coherent spontaneous BOLD fluctuations persist during the anaesthetized state. All subsequently presented results represent data acquired over multiple BOLD runs in multiple animals at isoflurane levels between 0.8% and 1.5%. Group-averaged ($N = 8$) statistical maps for each oculomotor seed ROI are shown in Supplementary Fig. 1. Conjunction analyses of these data demonstrated that FEF, LIP, middle temporal (MT) and middle superior temporal (MST) areas were consistently correlated with all oculomotor seed ROIs (Fig. 2a and Supplementary Fig. 1e).

To determine the system specificity of coherent spontaneous BOLD fluctuations, additional seed ROIs were anatomically defined in left and right somatomotor cortex (SMC; see Supplementary Fig. 2). Regional time courses of BOLD fluctuations were extracted from all

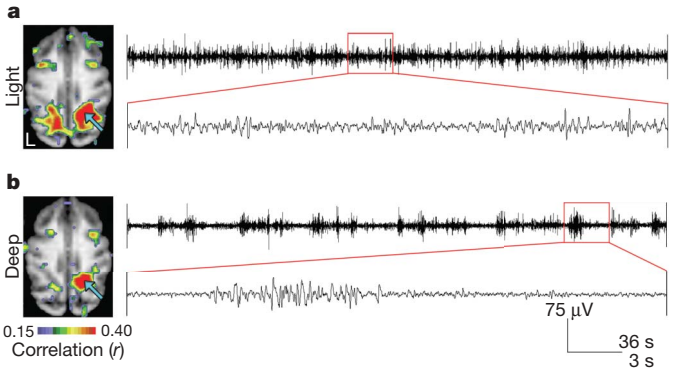

Figure 1 | BOLD correlation maps obtained at two levels of isoflurane anaesthesia in one monkey. Correlation maps computed with a seed region in right LIP (blue arrows) are superimposed on a structural MRI. Simultaneously recorded EEG is shown to the right of each correlation map. In both **a** and **b**, the top and bottom traces show 360 and 30 s of EEG, respectively. **a**, 0.90% isoflurane; continuous, slow EEG activity. L, left side. **b**, 1.25% isoflurane; burst suppression EEG pattern. The principal components of the cortical oculomotor system (bilateral FEF, bilateral LIP) are present in the correlation maps during both light (**a**) and deep (**b**) anaesthesia (defined electrophysiologically). A more systematic examination of the dependence of BOLD correlations on level of anaesthesia is given in Supplementary Figs 4–6.

[1]Departments of Radiology, [2]Neurology, [3]Anatomy and Neurobiology, and [4]Biomedical Engineering, Washington University in St Louis, Missouri 63110, USA. [5]Department of Psychology, Center for Brain Science, Harvard University, Cambridge, Massachusetts 02138, USA. [6]Athinoula A. Martinos Center for Biomedical Imaging, Massachusetts General Hospital, Charlestown, Massachusetts 02129, USA.

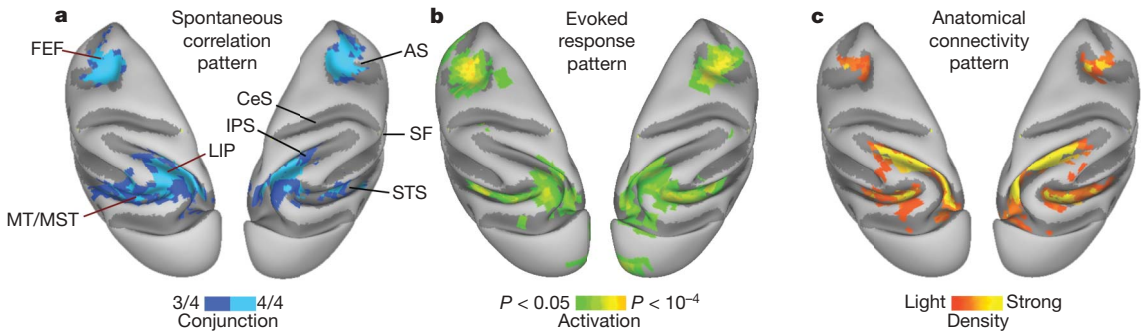

Figure 2 | Cortical patterns of coherent spontaneous BOLD fluctuations are similar to those of task-evoked responses and anatomical connectivity. **a**, Conjunction map of BOLD correlations within the oculomotor system on dorsal views of the monkey atlas left and right hemisphere surfaces (same data as Supplementary Fig. 1e). Voxels significantly correlated with three (dark blue) or four (light blue) oculomotor ROIs are shown. **b**, Activation pattern evoked by performance of a saccadic eye movement task (average of two monkeys; adapted from ref. 9). **c**, Density of cells labelled by retrograde tracer injections into right LIP (average of three monkeys; adapted from ref. 10). The left hemisphere injection data are duplicated by reflection of the right hemisphere to facilitate visual comparison. Only regions that showed reproducible projections to LIP (three out of three monkeys) are shown. AS, arcuate sulcus; CeS, central sulcus; IPS, intraparietal sulcus; SF, sylvian fissure; STS, superior temporal sulcus. Data are available at http://sumsdb.wustl.edu/sums/directory.do?id=6602646.

oculomotor and somatomotor ROIs and cross-correlated (Supplementary Fig. 3a). Spontaneous BOLD fluctuations were robustly temporally correlated between each pair of oculomotor ROIs (two-tailed t-test, all $P < 0.05$) and similarly correlated between the left and right somatomotor ROIs ($P < 0.05$). Critically, none of the oculomotor ROIs was significantly correlated with either the left or right somatomotor cortex (all $P > 0.1$). An additional analysis tested the degree to which correlation maps derived from various ROIs were spatially similar[8] (Supplementary Fig. 3b). All correlation maps corresponding to ROIs within the oculomotor system were spatially correlated (two-tailed t-test, all $P < 0.05$) as were the maps corresponding to the left and right SMC ($P < 0.05$). Notably, none of the correlation maps derived from the oculomotor ROIs was spatially correlated with the maps derived from the somatomotor ROIs (all $P > 0.1$).

To examine the similarity between task-evoked and spontaneous BOLD correlation patterns, we compared the map of spontaneous oculomotor system correlations to a map of BOLD responses evoked during performance of a saccadic eye movement task in two awake monkeys (data from ref. 9). Figure 2a, b demonstrates that the pattern of saccade task-evoked activations resembles the distribution of spontaneous BOLD correlations in the oculomotor system, which is confirmed by significant spatial correlations between the saccade task-evoked response map and the spontaneous BOLD correlation maps derived from each oculomotor ROI (two-tailed t-test, all $P < 10^{-4}$). These results suggest that the systems showing coherent spontaneous BOLD fluctuations under anaesthesia are similar to systems commonly engaged concurrently during task performance in awake animals.

To evaluate whether the correlation structure of spontaneous BOLD fluctuations relates to the underlying anatomical circuitry, we compared the present oculomotor system correlation maps to a previous study[10] of retrograde tracer injections into area LIP. Figure 2c shows the density of retrogradely labelled cortical cells (averaged across three monkeys) projected onto the cortical surface. A marked similarity is evident in panels a and c of Fig. 2, which is confirmed by significant spatial correlations between the retrograde tracer map and

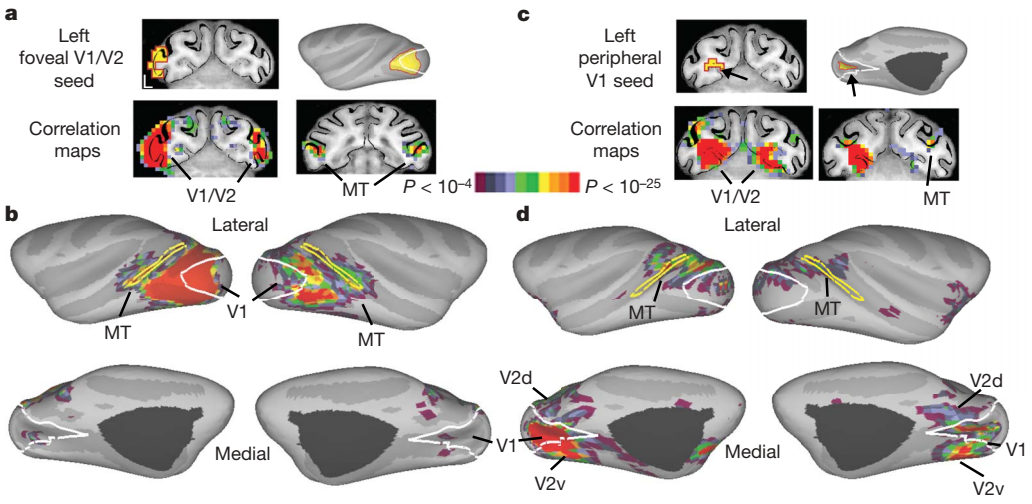

Figure 3 | Spontaneous BOLD correlations are topographically organized in the visual cortex of anaesthetized monkeys ($N = 8$). **a**, Left foveal V1/V2 ROI (yellow) on a coronal slice (upper left) and inflated surface (upper right). Correlation maps on coronal slices demonstrate correlations in contralateral foveal V1 and V2 (lower left) and bilaterally in and near area MT (lower right). **b**, Correlations displayed on inflated views of left and right hemispheres are stronger in regions representing the fovea compared with the periphery in visual areas V1, V2 and MT, based on published topographic maps[11,29,30]. **c**, Left peripheral V1 ROI (yellow, upper panels). Coronal slice views demonstrate correlations in contralateral peripheral V1 and V2 (lower left) and bilaterally in area MT (lower right). **d**, Correlations displayed on inflated views are stronger in peripheral compared with foveal representations in V1, V2 and MT. See Supplementary Fig. 7 for analogous results for the right hemisphere seed ROIs. Data are available at http://sumsdb.wustl.edu/sums/directory.do?id=6602646.

the spontaneous BOLD correlation maps derived from each oculomotor ROI (two-tailed *t*-test, all $P < 10^{-4}$).

To test further the relation to known anatomical circuitry, we analysed correlation patterns associated with retinotopically restricted regions of visual cortex. A left foveal V1/V2 ROI revealed a marked pattern of bilateral correlations in the superior temporal sulcus in and near ventral MT, where the fovea is represented[11] (Fig. 3a, b). Contralateral correlations were stronger in V2 than in V1 and in the foveal representation compared with the visual periphery. In contrast, a peripheral V1 ROI (within the calcarine sulcus) revealed bilateral correlations that were stronger in and near dorsal MT (representing the periphery) than in ventral MT and were stronger in peripheral compared with foveal V1/V2 (Fig. 3c, d). Thus, the correlation structure of spontaneous BOLD fluctuations in visual cortex exhibits sub-areal, retinotopic organization. Given the absence of direct interhemispheric connections involving V1 away from the vertical meridian[12], the correlations in contralateral V1 must be sustained by polysynaptic pathways that respect visual retinotopy along the eccentricity axis. Additional discussion of relations between anatomical and functional connectivity is given in Supplementary Note 1.

The above results concern systems that are well known in both monkeys and humans. However, there exists a set of regions that is commonly deactivated during attention-demanding cognitive tasks (the so-called 'default' system[13]) that, heretofore, has been described only in humans. The default system is posited to support higher mental faculties including understanding others' mental states[14], self-referential behaviour[15], moral reasoning[16], recollection[17] and imagining the future[18]. Many of these behaviours have been proposed to be uniquely human[19]. Although anatomical tract tracing results suggest that elements of a similar system may exist in the monkey[20], some components of the human default system reside in areas (specifically, Brodmann areas 39 and 40) that have no clear homologue in the monkey brain[21,22].

In humans, spontaneous fluctuations within the default system are robustly correlated with the posterior cingulate/precuneus cortex (pC/PCC)[3,4]. We examined the spontaneous BOLD correlations associated with the monkey pC/PCC (defined anatomically) to determine whether a similar system exists in the monkey. Regions significantly correlated with the pC/PCC in anaesthetized monkeys included dorsal medial prefrontal cortex, lateral temporoparietal cortex (including area 7a and superior temporal gyrus) and posterior parahippocampal cortex (Fig. 4a). Figure 4b shows the analogous result obtained in ten humans scanned in a resting state (see Methods). The resemblance between the monkey and human pC/PCC correlation maps suggests that many elements of the default system may be conserved across primate species. More speculatively, the similarity of the pC/PCC correlation with lateral temporoparietal cortex in both species suggests a potential homologue of human areas 39 and 40 in the macaque. Future research may reveal whether the systems illustrated in Fig. 4 have similar functions across species (see Supplementary Note 2).

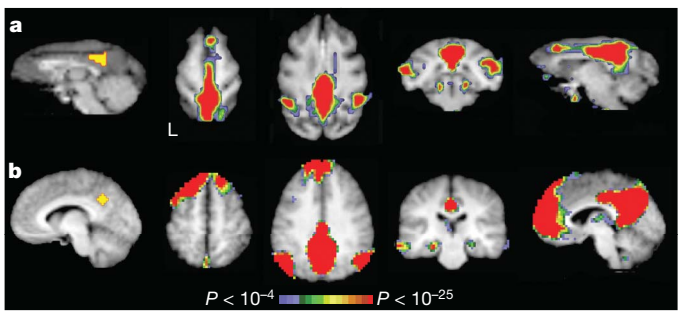

Figure 4 | Significant voxel-wise correlations of the pC/PCC in monkey and human. The seed ROI used in each species is shown on the left. **a**, Data from eight anaesthetized monkeys. **b**, Data from ten resting humans.

Our results demonstrate that cortical systems previously associated with the performance of sensory, motor, and/or cognitive tasks are manifest in the correlation structure of spontaneous BOLD fluctuations observed in the absence of normal perception or behaviour. Thus, coherent spontaneous BOLD fluctuations cannot exclusively be a reflection of conscious mental activity[7], but may reflect a more fundamental or intrinsic property of functional brain organization. These findings are consistent with the perspective that the brain is governed primarily by internal dynamics[23–28]. Furthermore, our findings introduce a new approach for comparing the functional architecture of the brain across species.

METHODS SUMMARY

fMRI was acquired in 11 anaesthetized adult macaque monkeys (eight *Macaca fascicularis*; three *Macaca mulatta*). Protocols for anaesthesia and magnetic resonance imaging were reviewed and approved by the Animal Studies Committees of Washington University. Each monkey was initially chemically restrained with ketamine (10 mg kg^{-1} for *M. mulatta*; 15 mg kg^{-1} for *M. fascicularis*) and atropine (0.05 mg kg^{-1}) to decrease bronchial and salivary secretions. After intubation, anaesthesia was maintained for the duration of the scan with isoflurane (0.8–1.5%). The anaesthetic level was adjusted to eliminate responses (somatic movement or cardiac rate change) to toe pinches while keeping the heart rate above 70 beats per minute. Corneal reflexes were absent at all times. Neuromuscular blockade was not used. Four monkeys were scanned with simultaneous EEG and fMRI; eight monkeys were scanned without simultaneous EEG. One monkey was used in both studies. Between 6 and 23 BOLD runs of 300 functional volumes (~15 min run^{-1}) were acquired in each monkey. Pre-processing of fMRI data and analysis of spontaneous BOLD correlations was performed as previously described[3,6,8]. The BOLD time course in functionally and anatomically defined ROIs was correlated with the time course in other ROIs and with the time course at each brain voxel to create spontaneous BOLD fluctuation correlation maps. Surface representations were created using Caret software (http://brainmap.wustl.edu/caret/). Correlation maps representing the oculomotor system were compared to maps of saccadic eye-movement-evoked fMRI responses[9], anatomical connectivity maps determined by ventral LIP retrograde tracer injections[10], and correlation maps obtained in ten adult humans performing continuous fixation[3,6,8].

Full Methods and any associated references are available in the online version of the paper at www.nature.com/nature.

Received 28 November 2006; accepted 14 March 2007.

1. Raichle, M. E. & Mintun, M. A. Brain work and brain imaging. *Annu. Rev. Neurosci.* **29,** 449–476 (2006).
2. Biswal, B., Yetkin, F. Z., Haughton, V. M. & Hyde, J. S. Functional connectivity in the motor cortex of resting human brain using echo-planar MRI. *Magn. Reson. Med.* **34,** 537–541 (1995).
3. Fox, M. D. *et al.* The human brain is intrinsically organized into dynamic, anticorrelated functional networks. *Proc. Natl Acad. Sci. USA* **102,** 9673–9678 (2005).
4. Greicius, M. D., Krasnow, B., Reiss, A. L. & Menon, V. Functional connectivity in the resting brain: a network analysis of the default mode hypothesis. *Proc. Natl Acad. Sci. USA* **100,** 253–258 (2003).
5. Damoiseaux, J. S. *et al.* Consistent resting-state networks across healthy subjects. *Proc. Natl Acad. Sci. USA* **103,** 13848–13853 (2006).
6. Vincent, J. L. *et al.* Coherent spontaneous activity identifies a hippocampal-parietal memory network. *J. Neurophysiol.* **96,** 3517–3531 (2006).
7. Morcom, A. M. & Fletcher, P. C. Does the brain have a baseline? Why we should be resisting a rest. *Neuroimage* (in the press).
8. Fox, M. D., Corbetta, M., Snyder, A. Z., Vincent, J. L. & Raichle, M. E. Spontaneous neuronal activity distinguishes human dorsal and ventral attention systems. *Proc. Natl Acad. Sci. USA* **103,** 10046–10051 (2006).
9. Baker, J. T., Patel, G. H., Corbetta, M. & Snyder, L. H. Distribution of activity across the monkey cerebral cortical surface, thalamus and midbrain during rapid, visually guided saccades. *Cereb. Cortex* **16,** 447–459 (2006).
10. Lewis, J. W. & Van Essen, D. C. Corticocortical connections of visual, sensorimotor, and multimodal processing areas in the parietal lobe of the macaque monkey. *J. Comp. Neurol.* **428,** 112–137 (2000).
11. Maunsell, J. H. & Van Essen, D. C. Topographic organization of the middle temporal visual area in the macaque monkey: representational biases and the relationship to callosal connections and myeloarchitectonic boundries. *J. Comp. Neurol.* **266,** 535–555 (1987).
12. Van Essen, D. C., Newsome, W. T. & Bixby, J. L. The pattern of interhemispheric connections and its relationship to extrastriate visual areas in the macaque monkey. *J. Neurosci.* **2,** 265–283 (1982).

13. Raichle, M. E. *et al.* A default mode of brain function. *Proc. Natl Acad. Sci. USA* **98,** 676–682 (2001).
14. Saxe, R. & Kanwisher, N. People thinking about thinking people. The role of the temporo-parietal junction in ''theory of mind''. *Neuroimage* **19,** 1835–1842 (2003).
15. Vogeley, K. & Fink, G. R. Neural correlates of the first-person-perspective. *Trends Cogn. Sci.* **7,** 38–42 (2003).
16. Greene, J. D., Sommerville, R. B., Nystrom, L. E., Darley, J. M. & Cohen, J. D. An fMRI investigation of emotional engagement in moral judgment. *Science* **293,** 2105–2108 (2001).
17. Wagner, A. D., Shannon, B. J., Kahn, I. & Buckner, R. L. Parietal lobe contributions to episodic memory retrieval. *Trends Cogn. Sci.* **9,** 445–453 (2005).
18. Addis, D. R., Wong, A. T. & Schacter, D. L. Remembering the past and imagining the future: Common and distinct neural substrates during event construction and elaboration. *Neuropsychologia* **45,** 1363–1377 (2007).
19. Tulving, E. in *The Missing Link in Cognition: Origins of Self-Reflective Consciousness* (eds Terrace, H. S. & Metcalfe, J.) 3–56 (Oxford Univ. Press, New York, 2005).
20. Suzuki, W. A. & Amaral, D. G. Perirhinal and parahippocampal cortices of the macaque monkey: cortical afferents. *J. Comp. Neurol.* **350,** 497–533 (1994).
21. Karnath, H.-O. New insights into the functions of the superior temporal cortex. *Nature Rev. Neurosci.* **2,** 568–576 (2001).
22. Brodmann, K. *Localisation in the Cerebral Cortex* (Smith-Gordon, London, 1994).
23. MacLean, J. N., Watson, B. O., Aaron, G. B. & Yuste, R. Internal dynamics determine the cortical response to thalamic stimulation. *Neuron* **48,** 811–823 (2005).
24. Llinas, R. *I of the Vortex: From Neurons to Self* (MIT Press, Cambridge, Massachusetts, 2001).
25. Buzsaki, G. & Draguhn, A. Neuronal oscillations in cortical networks. *Science* **304,** 1926–1929 (2004).
26. Kenet, T., Bibitchkov, D., Tsodyks, M., Grinvald, A. & Arieli, A. Spontaneously emerging cortical representations of visual attributes. *Nature* **425,** 954–956 (2003).
27. Raichle, M. E. Neuroscience. The brain's dark energy. *Science* **314,** 1249–1250 (2006).
28. Fiser, J., Chiu, C. & Weliky, M. Small modulation of ongoing cortical dynamics by sensory input during natural vision. *Nature* **431,** 573–578 (2004).
29. Van Essen, D. C., Newsome, W. T. & Maunsell, J. H. The visual field representation in striate cortex of the macaque monkey: asymmetries, anisotropies, and individual variability. *Vision Res.* **24,** 429–448 (1984).
30. Gattass, R., Sousa, A. P. & Gross, C. G. Visuotopic organization and extent of V3 and V4 of the macaque. *J. Neurosci.* **8,** 1831–1845 (1988).

Supplementary Information is linked to the online version of the paper at www.nature.com/nature.

Acknowledgements We thank J. L. Price, J. S. Perlmutter and G. C. DeAngelis for discussion and for allowing us to scan their monkeys; L. J. Larson-Prior for providing the human data; J. Harwell for Caret software enhancements used in data analysis; and K. J. Black for providing the monkey atlas target. Grants from the US National Institute of Health, US National Science Foundation, Washington University Silvio Conte Center, and Mallinckrodt Institute of Radiology supported these studies.

Author Information Reprints and permissions information is available at www.nature.com/reprints. The authors declare no competing financial interests. Correspondence and requests for materials should be addressed to M.E.R. (marc@npg.wustl.edu).

METHODS

Subjects and data acquisition: monkeys. Eleven healthy adult macaque monkeys (eight *Macaca fascicularis*; three *Macaca mulatta*) were used in this study. Protocols for anaesthesia and magnetic resonance imaging were reviewed and approved by the Animal Studies Committee of Washington University. Each animal was initially chemically restrained with ketamine (10 mg kg^{-1} for *M. mulatta*; 15 mg kg^{-1} for *M. fascicularis*) and administered atropine (0.05 mg kg^{-1}) to decrease bronchial and salivary secretions. After intubation, anaesthesia was maintained for the duration of the scan with isoflurane (0.8–1.5%). The anaesthetic level was adjusted to eliminate responses (somatic movement or cardiac rate change) to toe pinches while keeping the heart rate above 70 beats per minute. Corneal reflexes were consistently absent at all times. Neuromuscular blockade was not used. Four monkeys were scanned with simultaneous EEG and fMRI; eight monkeys were scanned without simultaneous EEG. One monkey participated in both studies.

The four monkeys in the EEG–fMRI experiments were initially maintained at 0.8–1.1% isoflurane for between 8 and 15 BOLD runs and then at the higher level of 1.2–1.5% for between 8 and 22 runs. Electrophysiological depth of anaesthesia was monitored throughout scanning by an expert electroencephalographer (J.M.Z.) and graded according to the EEG pattern: continuous low frequency activity was defined as light anaesthesia whereas a clear burst suppression pattern was defined as deep anaesthesia.

Magnetic resonance scanning was performed at the Washington University School of Medicine using a 3T Allegra scanner (Siemens). fMRI data were acquired using a gradient-echo echo-planar sequence sensitive to BOLD contrast (volume repetition time (TR) = 3.02 s, T2* evolution time (TE) = 25 ms, flip angle = 90°, 1.5 mm^2 in plane resolution, slice thickness = 1.6 mm). Two monkeys were scanned using a surface coil; the remaining monkeys were scanned using a volumetric coil (both coils from Primatrix). In three monkeys, each whole-brain volume consisted of 52 coronal slices. In the remaining monkeys, each volume consisted of 52 sagittal slices. In all monkeys, the slices were acquired using contiguous, interleaved acquisition. Between 6 and 23 BOLD runs of 300 functional volumes (300 volumes are approximately 15 min) were acquired in each monkey. Sagittal, high-resolution, T1-weighted, magnetization-prepared rapid gradient echo (MP-RAGE) structural images were also acquired (TR = 1.85 s; TE = 3.93 ms, flip angle = 7°, 0.5 mm^3 voxels) and used to align the functional data to a monkey atlas[31,32].

Electroencephalograms were recorded using a MagLink (Compumedics Neuroscan) system equipped with a 24-bit Synamps/2 DC amplifier. The mastoid, VEOG and EKG electrodes (sintered Ag/AgCl) of the MagLink cap were attached to the head of the monkey using collodion. The right and left posterior electrodes were placed 2 cm anterior and lateral to the inion with the right and left anterior electrodes 3 cm anterior to the posterior electrodes. The reference electrode was placed on the midline 3 cm anterior to the anterior electrodes and the ground was placed 2 cm to the left of the reference electrode. All electrode leads were carbon fibre in series with a current limiting resistor for subject safety. Electrode impedances were kept below 10 kΩ. Scan 4.3 Acquire (Compumedics Neuroscan) was used to record EEG both in referential and bipolar modes at a 20 KHz sampling rate (rate needed for subsequent gradient artefact reduction). In general, EEG recorded in a bipolar configuration was of higher quality. EKG was recorded using a bipolar derivation (Millenium monitor, InVivo Research). The electrophysiological data were band-pass filtered (1–20 Hz, 48 dB roll-off) and magnetic resonance gradient artefact was effectively eliminated using Scan 4.3 Edit (Compumedics Neuroscan). The gradient-artefact-reduced electrophysiological data were then decimated to 500 Hz. Ballistocardiogram was reduced using in-house software[33].

Subjects and data acquisition: humans. Ten normal right-handed human participants (mean age = 23.2 ± 2.6 yr; four males) underwent three 5.5-min fMRI scans (Siemens Allegra) during maintained visual fixation. Additional technical details are given in previous reports in which these data were used to study spontaneous BOLD fluctuations[3,6,8].

Processing of imaging data. For both species, the fMRI pre-processing steps included: first, compensation of systematic, slice-dependent time shifts; second, elimination of systematic odd-even slice intensity differences due to interleaved acquisition; and third, rigid-body correction for inter-volume head motion within and across runs. Step three provided a record of head position within and across all fMRI runs. Each fMRI run was intensity scaled (one multiplicative constant over all voxels and functional volumes) to yield a whole brain mode value of 1,000 (not counting the first four functional volumes)[34]. Atlas registration was achieved by computing affine transforms connecting the fMRI run first functional volume (averaged over all runs after cross-run realignment) with the average T1-weighted structural images[34]. Our macaque atlas representative template includes MP-RAGE data from 11 normal cynomolgus monkeys and was made to conform to the 2000 Martin and Bowden atlas[35] (see http://www.purl.org/net/kbmd/cyno). Our human atlas representative template includes MP-RAGE data from 12 normal individuals and was made to conform to the 1988 Talairach atlas[36] according to the method of ref. 37.

To prepare the BOLD data for the present main analyses, each fMRI run was transformed to atlas space. The human BOLD data were resampled to 3-mm cubic voxels. The monkey BOLD data were resampled to 1.5-mm cubic voxels. This step combined movement correction within and across runs and atlas transformation in a single resampling.

Several processing steps were used to condition the functional data for analysis of voxel-based correlations as described previously[3,6]. Monkey and human data were temporally filtered to retain frequencies in the $0.0025 < f < 0.05$ Hz and $0.009 < f < 0.08$ Hz bands, respectively. The monkey and human data were spatially smoothed with 3 mm and 6 mm full-width at half-maximum (FWHM) gaussian kernels, respectively. Several sources of spurious variance were removed from the time series by regression of nuisance variables and their temporal derivatives: (1) six parameters obtained by rigid-body correction of head motion; (2) the whole-brain signal averaged over a fixed region in atlas space. The humans also had the signal from a ventricular region of interest and a region centred in the white matter removed. This regression procedure removes fluctuations unlikely to represent regionally specific correlations of neuronal origin.

Creation of ROIs. Monkey oculomotor ROIs were defined from a previous study of saccadic eye movements[9]. Activation maps were assigned a threshold at a significance level of $P < 0.05$ (fixed effects analysis). ROIs included all contiguous voxels surrounding the most significantly activated peak around left and right LIP and FEF. The LIP ROIs included activated voxels on the lateral bank of the intraparietal sulcus. The FEF ROIs included activated voxels on the anterior bank of the arcuate sulcus. In addition, left and right somatomotor cortex ROIs were defined around Brodmann area 4 according to the partitioning scheme of ref. 38, registered from F99 atlas to the present F6 cortical surface (see 'Surface-based mapping' below). The monkey posterior cingulate/precuneus cortex (pC/PCC) ROI was anatomically defined according to the atlas of ref. 35. Similarly, the ROIs for visual topographic subregions were delineated using the partitioning scheme of ref. 38 for areas V1 and V2 and known topographic organization of V1 and V2[29]. The oculomotor, somatomotor and visual ROIs were drawn on the atlas cortical surface, and then mapped to voxels within 1.5 mm of the specified surface nodes.

The human posterior cingulate/precuneus was defined as a 12-mm-diameter sphere centred on a peak focus from a meta-analysis of default activity (Talairach coordinates: −7, −53, 34)[39].

Regional correlations. Pearson correlation coefficient between region pairs were computed as

$$r_{xy} = \frac{(1/T)\sum_{t=1}^{T}[x(t)-\bar{x}]\cdot[y(t)-\bar{y}]}{s_x s_y}$$

where $x(t)$ and $y(t)$ are the regional time courses with means $\bar{x}$ and $\bar{y}$, respectively, and standard deviations s_x and s_y, respectively. The summation limit, T, corresponds to the total number of time points in multiple, concatenated BOLD runs, excluding the first four (pre-magnetization steady state) functional volumes of each run.

Correlation mapping. For each subject and each ROI, correlation maps were computed as previously described[2,3,6] by correlating a selected regional time course, $x(t)$, against all other voxels in the brain. Thus,

$$r_x(v) = \frac{(1/T)\sum_{t=1}^{T}[x(t)-\bar{x}]\cdot[I(v,t)-\bar{I}(v)]}{s_x s_{I(v)}}$$

where $I(v,t)$ represents the time course at locus v and time t with mean $\bar{I}(v,t)$ and standard deviation $s_{I(v)}$. The coefficient $r_x(v)$ is the correlation between the time course at voxel v and the regional time course, $x(t)$.

Application of Fisher's z transform[40]

$$z(v) = 0.5\ln\left(\frac{1+r(v)}{1-r(v)}\right)$$

yielded maps with values at each voxel that theoretically are nearly normally distributed over the population of subjects.

Fixed effects significance maps were created for each individual by converting $z(v)$ maps to Z score maps (that is, zero mean, unit variance, gaussian distributions under the null hypothesis of no correlation). Thus, $z(v)$ was divided by the square root of the theoretical variance, computed as $1/\sqrt{(n-3)}$ where n is the degrees of freedom. To account for autocorrelation in the BOLD signal according to Bartlett's theory, n was taken as the total number of time points (functional volumes) used to compute $z(v)$, divided by the time integral of the square of the lagged autocorrelation function[41]. Z score maps were combined across subjects

using a fixed-effects analysis (sum and divide by the square root of number of subjects) to generate group Z score maps. The group Z score maps were converted to maps of probability for display in Figs 3 and 4 and Supplementary Figs 1, 2 and 7. All statistical maps were corrected for multiple comparisons using a stringent Bonferroni correction (proportional to total number of brain voxels) and a threshold set at $P < 10^{-4}$. These group statistical maps were used to compute conjunction maps.

Conjunction maps. Conjunction maps were used to visualize voxels consistently correlated with all ROIs within a spontaneously emerging functional system (for example, the four oculomotor ROIs). Conjunction maps were computed on the basis of the Bonferroni corrected group statistical maps. Thus, at each voxel, the number of group statistical maps that were significant at the $P < 10^{-4}$ level were counted. Voxels meeting this criterion for 3 out of 4 oculomotor ROIs are displayed in Fig. 2a and Supplementary Fig. 1e. A somatomotor system conjunction map is shown in Supplementary Fig. 2c.

Conjunction maps were also used in Supplementary Fig. 5 to illustrate voxels consistently correlated with multiple ROIs within the oculomotor and somatomotor systems during anaesthesia. Descriptive rather than hypothesis testing statistics were used to facilitate comparisons across levels of anaesthesia. Thus, these maps were constructed by voxel-wise counting of the number of group $r(v)$ maps with mean correlation $(r) \geq 0.07$.

Evaluation of map similarity: spatial correlation. Similarity of spatial distribution was evaluated for several types of maps (spontaneous BOLD correlation maps, task-evoked BOLD response maps, and anatomical connectivity maps) by computing the standard Pearson correlation coefficient over all voxels within the brain[8]. To evaluate similarity of BOLD fluctuation correlation maps, the Pearson formula was applied after Fisher's transformation (that is, on the basis of $z(v)$). Thus, for correlation maps corresponding to ROIs x and y,

$$R_{xy} = \frac{\sum_{v=1}^{V} [z_x(v) - \bar{z}_x] \cdot [z_y(v) - \bar{z}_y]}{\sqrt{\sum_{v=1}^{V} [z_x(v) - \bar{z}_x]^2} \cdot \sqrt{\sum_{v=1}^{V} [z_y(v) - \bar{z}_y]^2}}$$

where all summations are taken over all voxels within the brain. The capitalized 'R' denotes the spatial correlation coefficient whereas the lowercase 'r' is used for temporal correlation. To generate the results shown in Supplementary Fig. 3b, the spatial correlation coefficient for each pair of $z(v)$ maps was first computed for all individuals. The individual R_{xy} values then were converted to Fisher z values and averaged. Statistical significance was tested using a two-tailed t-test over subjects (random effects analysis) against the null hypothesis of no spatial correlation.

Comparison of spontaneous, evoked and anatomical connectivity patterns. The distribution of BOLD responses evoked by performance of a saccadic eye movement task was obtained in the form of a Z score map from a previous fMRI study of awake behaving monkeys[9]. The similarity between this map and maps of coherent spontaneous activity were independently evaluated for several ROIs (left and right FEF, LIP and somatomotor cortex) using the above-described spatial correlation coefficient. The strategy used to combine map similarity measures across subjects and to evaluate statistical significance was as described above in connection with evaluating similarity of correlation maps. Thus, the spatial correlation coefficient was computed in individuals and converted to Fisher's z. Statistical significance was determined at the group level using a two-tailed t-test against the null hypothesis of no spatial correlation.

Ventral LIP anatomical connectivity data[10] (cases B, C and D) were downloaded from the Surface Management Systems DataBase (http://sumsdb.wustl.edu:/sums/directory.do?id=679531). These monkeys had retrograde tracer injections (Fast Blue, Sigma, 5% aq.) into ventral LIP. At least 50% of tracer uptake was within ventral LIP; some tracer was also present in the lateral ventral intraparietal area (VIP) in two of the monkeys. For each monkey, the Caret surface metric file containing the density of retrogradely labelled cells was exported as a volume with the same resolution as the atlas-transformed fMRI data ($1.5 \times 1.5 \times 1.5$ mm).

Areas consistently labelled with tracer in all three monkeys were identified by counting, at each voxel, the number of cases containing label. Voxels meeting this criterion in three out of three cases were used as mask for an image of the voxel-wise density of cells labelled by the tracer (averaged over the three cases). This image was re-projected onto a cortical surface representation for display (Fig. 2c). Similarity of LIP anatomical connectivity to spontaneous BOLD correlation maps was independently evaluated for several correlation maps (corresponding to left and right FEF, LIP and somatomotor cortex ROIs) exactly as described above in connection with the saccade task-evoked response map.

Surface-based mapping. To create a surface map of the monkey cortex, T1-weighted MP-RAGE anatomical images of six monkeys (*M. fascicularis*) were mutually co-registered and averaged using a previously described iterative scheme[31,42] and a reference target[32] representing the atlas of ref. 35 (see http://www.purl.org/net/kbmd/cyno). This image then was segmented for the creation of a flattened cortical surface map using the Caret software suite[43] to create the 'F6' macaque cortical surface atlas. A nonlinear landmark-driven procedure was used to register the cortical surface to a surface-based monkey brain atlas (F99UA1, http://sumsdb.wustl.edu:/sums/directory.do?id=679531). Cortical area boundaries established from a previous study were used to assign correlations to specific cortical regions for descriptive purposes[38].

The functional correlation maps in Fig. 3 were projected from volume data to F6 atlas surface using the Caret 'average voxel' method with a 1.5-mm averaging radius. This extent was needed in order to capture significant functional data that were slightly misaligned with the structural MRI volume and the atlas surface owing to imperfect registration of the EPI data to the underlying structural MRI. Consequently, the atlas cortical surface maps are blurred as a result of this procedure as well as the initial pre-processing (spatial smoothing of 3 mm FWHM).

31. Black, K. J., Koller, J. M., Snyder, A. Z. & Perlmutter, J. S. Atlas template images for nonhuman primate neuroimaging: baboon and macaque. *Methods Enzymol.* **385,** 91–102 (2004).
32. Black, K. J., Koller, J. M. & Perlmutter, J. S. Template images for neuroimaging in *Macaca fascicularis*. Program No. 454.18. Abstract Viewer and Itinerary Planner ⟨http://www.purl.org/net/kbmd/cyno⟩ (Society for Neuroscience, Washington DC, 2005).
33. Vincent, J. L., Larson-Prior, L. J., Zempel, J. M. & Snyder, A. Z. Moving GLM ballistocardiogram artifact reduction for EEG data acquired simultaneously with fMRI. *Clin. Neurophysiol.* **118,** 981–998 (2007).
34. Ojemann, J. G. *et al.* Anatomic localization and quantitative analysis of gradient refocused echo-planar fMRI susceptibility artifacts. *Neuroimage* **6,** 156–167 (1997).
35. Martin, R. F. & Bowden, D. M. *Primate Brain Maps: Structure of the Macaque Brain* (Elsevier, Amsterdam, 2000).
36. Talairach, J. & Tournoux, P. *Co-planar Stereotaxic Atlas of the Human Brain* (Thieme Medical Publishers, New York, 1988).
37. Lancaster, J. L. *et al.* A modality-independent approach to spatial normalization of tomographic images of the human brain. *Hum. Brain Mapp.* **3,** 209–223 (1995).
38. Lewis, J. W. & Van Essen, D. C. Mapping of architectonic subdivisions in the macaque monkey, with emphasis on parieto-occipital cortex. *J. Comp. Neurol.* **428,** 79–111 (2000).
39. Shulman, G. L. *et al.* Common blood flow changes across visual tasks: II. Decreases in cerebral cortex. *J. Cogn. Neurosci.* **9,** 648–663 (1997).
40. Zar, J. H. *Biostatistical Analysis* (Prentice-Hall, Upper Saddle River, New Jersey, 1996).
41. Jenkins, G. M. & Watts, D. G. *Spectral Analysis and its Applications* (Emerson-Adams Press, Boca Raton, 1968).
42. Buckner, R. L. *et al.* A unified approach for morphometric and functional data analysis in young, old, and demented adults using automated atlas-based head size normalization: reliability and validation against manual measurement of total intracranial volume. *Neuroimage* **23,** 724–738 (2004).
43. Van Essen, D. C. *et al.* An integrated software suite for surface-based analyses of cerebral cortex. *J. Am. Med. Inform. Assoc.* **8,** 443–459 (2001).